

Birefringence dispersion study in $(C_{12}H_{25}NH_3)_2ZnCl_4$ crystal near its isotropic point

J. Fernández and R. Balda

Departamento de Física Aplicada, Escuela Técnica Superior de Ingenieros Industriales y de Telecomunicación, Universidad del País Vasco, E-48013 Bilbao, Spain

J. Etxebarria, M. A. Arriandiaga, and C. Socías

Departamento de Física, Facultad de Ciencias, Universidad del País Vasco, Apartado 644, E-48080 Bilbao, Spain

F. J. Jaque

Departamento de Física Aplicada, Facultad de Ciencias, Universidad Autónoma de Madrid, Cantoblanco, E-28049 Madrid 34, Spain

(Received 29 June 1987)

The optical dispersion in the organic-inorganic bis-dodecylammonium zinc tetrachloride $(C_{12}H_{25}NH_3)_2ZnCl_4$ crystal [in short, BAA(12)-ZnCl₄] around its isotropic point was investigated by means of birefringence and optical-absorption measurements. The birefringence dispersion data are analyzed with use of a simple oscillator model based on the optical band structure of BAA(12)-ZnCl₄. The adjustable parameters used for the theoretical birefringence are related with the oscillator strength and average position, respectively. The thermal behavior of the involved parameters is in accordance with the optical-absorption data obtained from the temperature dependence of the absorption edge. These results suggest the existence of a structural phase transition at 315 K.

I. INTRODUCTION

In the last few years an increasing interest has arisen on the study of perovskite-layer compounds, with the general formula $(C_nH_{2n+1}NH_3)_2MX_4$ [bis-(alkylammonium)MX₄, abbreviated hereafter as BAA-MX₄] related to the low-temperature magnetic order, structural phase transition sequences, and long-chain conformational changes.¹⁻⁵ This interest was recently reinforced by the detection of incommensurate phase transitions in BAA(3)-MnCl₄,⁶⁻¹⁰ and a pure and proper gyrotropic phase transition in BAA(5)-ZnCl₄.¹¹ Moreover, the existence of isotropic points together with a high optical dispersion were found in long-chain ($n=10,12,14$) BAA(n)-ZnCl₄ and BAA(n)-ZnCl₂Br₂,¹² and in the short-chain BAA(2)-CuCl₄ crystal.¹³

These optical properties open up new possibilities for the members of the BAA(n)-MX₄ family¹⁴ and lead us to look for an explanation to this singular behavior.

The wavelength and temperature dependence of the isotropic points, were extensively studied by some of the authors¹² by using conoscopic observation normal to the crystal plates, and measuring the acute apparent optical axial angle $2E$. For a given wavelength and starting at room temperature, $2E$ decreases as temperature increases, going finally to zero at some T_c (isotropic or uniaxial point temperature). At this point, on further heating, the optical plane rotates 90° and $2E$ starts to increase again. As we shall later see, this crossed axial plane dispersion appears to be a general feature related to the optical band structure and thermal and structural peculiarities of these layer crystals with aliphatic chains.

The aim of this paper is to study the optical dispersion in BAA(12)-ZnCl₄ around its isotropic point by means of birefringence measurements as a function of wavelength and temperature. Birefringence studies form an adequate basis for a quantitative approach because the wavelength of isotropy is clearly resolved in the birefringence dispersion curves. Moreover, birefringence data can be analyzed by means of a simple oscillator model based upon the optical band structure of the crystal. The adjustable parameters used for the birefringence parameterization show a good experimental fitting of the oscillator model and suggest the existence of a phase transition at 315 K.

The general features of the optical band structure are presented in Sec. II, and in Sec. III the oscillator model for the birefringence dispersion is described. The experimental results are shown in Sec. IV, and their discussion is presented in Sec. V.

II. THE OPTICAL BAND STRUCTURE

Long-chain BAA(n)-ZnCl₄ compounds have a pronounced two-dimensional structure of n -alkylammonium layers alternating with layers of isolated ZnCl₄ tetrahedra. The organic layer is formed by intercalated chains attached alternatively to both neighboring layers of ZnCl₄ units by weak hydrogen bonds from NH₃ groups to Cl ions,¹⁵ and the interlayer bonding is achieved by Van der Waals forces between the carbon chains as well as long-range Coulomb forces. In all these structures, the aliphatic chains always tend to organize in the most efficient way, and this is accomplished when each chain

is in the all-trans conformation and lies parallel to the others. This direction tends to be perpendicular to the ZnCl_4 layers.¹⁶ At room temperature the BAA(12)- ZnCl_4 crystal belongs to the monoclinic $P2_1/c$ space group with lattice parameters $a=10.379 \text{ \AA}$, $b=7.409 \text{ \AA}$, $c=44.399 \text{ \AA}$, and $\alpha=105.56^\circ$.¹⁷

The main characteristics of the energy band structure are well in accordance with these facts and support the principal role played by the ZnCl_4 tetrahedra. The optical absorption spectra of at BAA(12)- ZnCl_4 at room temperature obtained in the visible and near infrared regions show that the crystal is highly transparent as expected if electronic transitions are due to the ZnCl_4 units. Figure 1 presents the optical-absorption measurements in the ultraviolet region. As can be observed, an absorption peak is found at about 190 nm below the abrupt intense cutoff on the low-energy side of the fundamental absorption edge of the crystal. The low-energy side of the absorption peak shows an Urbach structure¹⁸⁻¹⁹ with a tail starting at about 230 nm at room temperature. Figure 2 shows the intensity of the peak as a function of temperature. This peculiar behavior can be explained by taking account of the covalent bonding effects between the chlorine and metal ions. The molecular orbital method seems to give the most realistic approach to the electronic structure of the compound. Figure 3 shows a simplified bonding scheme for a tetrahedral complex. The metal ion energy levels at the left interact with the ligand orbitals of the same symmetry type at the right to form the energy levels shown in the middle of the figure. The σ ligand orbital combinations transform according to the A_1 and T_2 representa-

tions of T_d and include both s and p orbitals. The π p -like ligand orbital combinations transform according to E , T_2 , and T_1 , whereas the $3d$ -like metal orbitals transform according to E and T_2 . The $4s$ -like metal orbital transforms according to A_1 and the $4p$ -like orbitals, according to T_2 .²⁰ As can be seen in Fig. 3 the two broad π, σ -like ligand orbitals are filled to completion, as well as the d -like metal levels $e(\pi^*) t(\sigma^*, \pi^*)$ which are occupied by the ten electrons coming from the Zn core. Excitation processes can induce transitions from the outer electronic configuration $t_1^6(\pi)$ of the π p -like filled ligand orbitals to the empty $a_1(\sigma^*)$ $4s$ -like metal level. From a group-theoretical point of view the (t_1^6) configuration of the electronic ground state is a singlet state 1A_1 , whereas the excited configuration $(t_1^5 a_1^1)$ can be a triplet 3T_1 or a singlet 1T_1 state. By symmetry arguments both transitions should be Laporte forbidden because in Td symmetry r transforms like T_2 . Moreover, for the triplet state the transition is also spin forbidden. The selection rules may, however, be released by the presence of the T_2 normal mode of vibration of the ZnCl_4 molecule. Thus, the coupling between the electronic and vibrational states allow for the observed dependence with temperature of the low energy side of the absorption peak. As mentioned before, the absorption coefficient exactly fits the Urbach rule¹⁸ $\alpha = \alpha_0 e^{g(h\nu - E_g)/kT}$ in the measured temperature range (g, α_0, E_g are adjustable constants and k is the Boltzmann's constant). The experimental fitting was made with $a = kT \ln \alpha_0 - gE_g$ and $b = g$ as adjustable parameters. Throughout the scanned temperature range, a

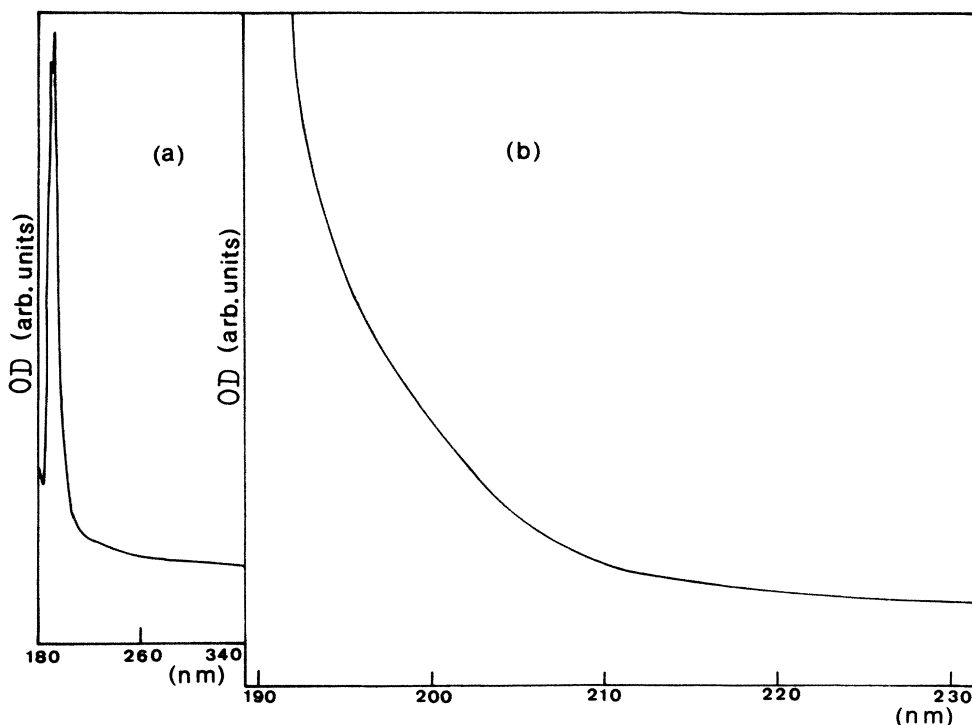


FIG. 1. Optical absorption measurements (OD optical density) in the ultraviolet region. (a) absorption peak at 190 nm. (b) detailed Urbach tail.

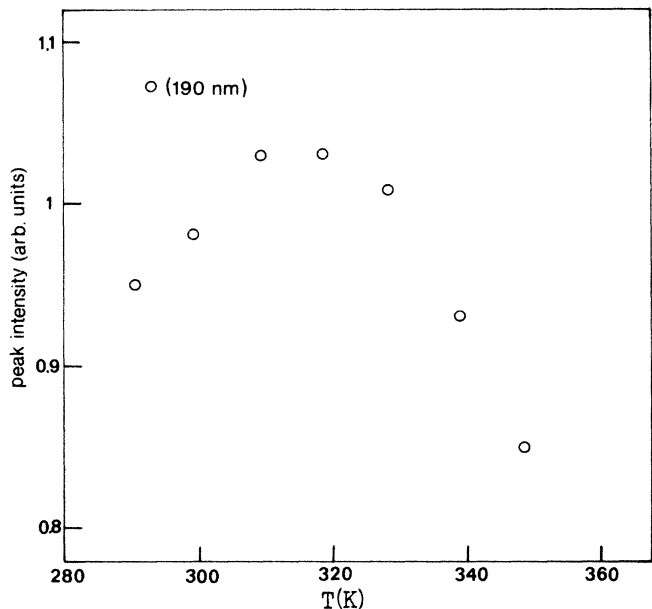


FIG. 2. Peak intensity as a function of temperature.

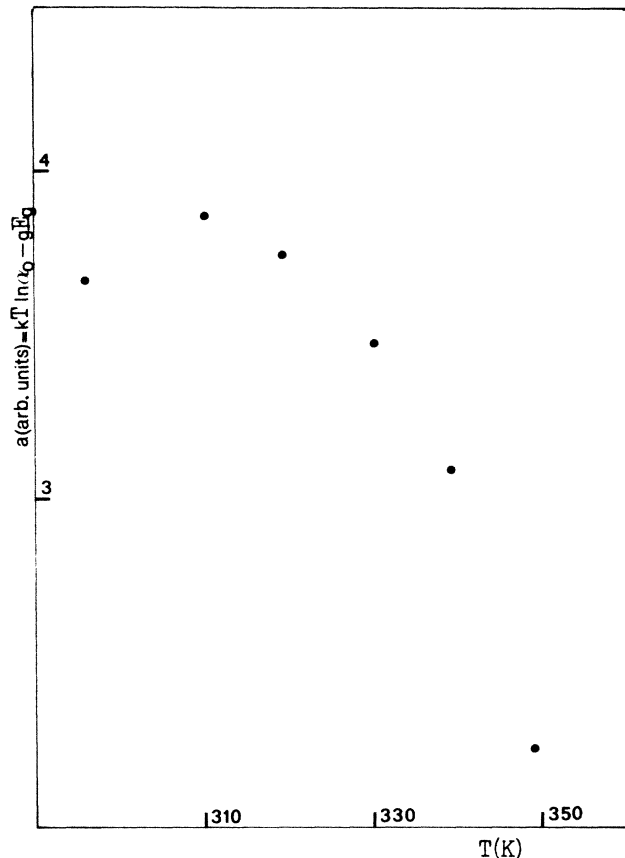


FIG. 4. Adjustable parameter as a function of temperature.

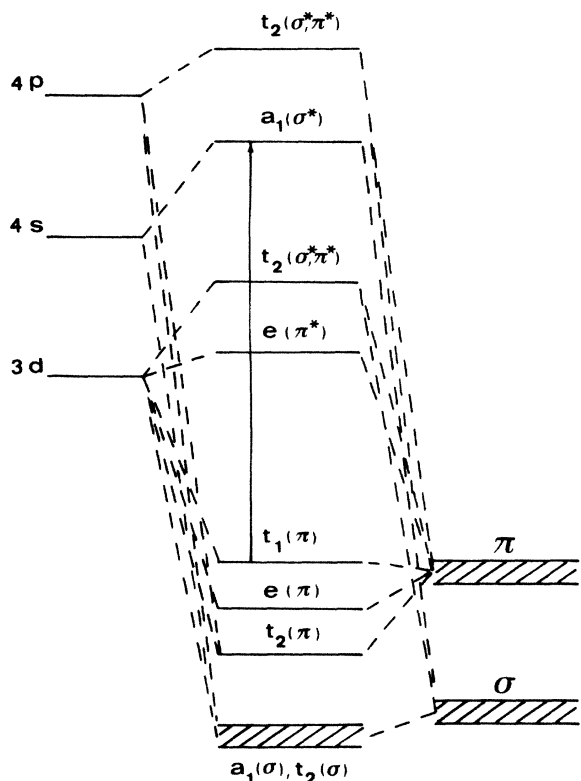


FIG. 3. A qualitative diagram showing the “ligand-metal” charge transfer transition involving the ground (t_1^0) and excited ($t_2^0 a_1$) configurations.

is found to be proportional to E_g . Figure 4 shows the variation of E_g as a function of temperature when the former simplification is made. Although no well-defined band gap can be found from an experimental edge, E_g roughly corresponds to the lowest peak of the absorption band.

III. OSCILLATOR MODEL OF THE BIREFRINGENCE DISPERSION

The dispersion behavior observed in BAA(12)-ZnCl₄ as temperature varies around the isotropic point is analyzed by means of a simple oscillator model (long wavelength approximation). If the incident light frequency is far from any of the resonance frequencies, and absorption is supposed to be negligible, then simple dispersion theory²¹ gives the index of refraction n of a dielectric medium as:

$$n^2(\omega) - 1 \approx \sum_i \frac{f_i}{\omega_i^2 - \omega^2} \tag{1}$$

where summation covers the individual dipole oscillator contributions from the selected optical bands, and ω_i and f_i are their resonance frequency and strength, respectively.

In terms of the wavelength this relation can be expanded for resonances lying in the low wavelength re-

gions giving the well known single term Sellmeier relation:

$$n^2(\lambda) - 1 = \frac{S_0 \lambda_0^2}{1 - (\lambda_0/\lambda)^2} \quad (2)$$

where λ_0 is some average oscillator position and S_0 is an average oscillator strength. In our case, if account is taken of the former description of the band structure of the material, the electronic transitions responsible for the observed optical absorption can be reasonably supposed to come from ZnCl_4 units. As the lowest absorption band below the fundamental absorption edge of the crystal is temperature dependent, a single average electronic oscillator with a temperature-dependent strength S and a position λ_0 has been chosen.

Then the birefringence associated to a section of the optical indicatrix defined by the n_b, n_a indices and parallel to the light vector E will be given by the expression:

$$\Delta n \approx \frac{\bar{\lambda}_0}{2\bar{n}} \left[\frac{\bar{\lambda}_0 \Delta S}{1 - \left(\frac{\bar{\lambda}_0}{\lambda}\right)^2} - \frac{2\bar{S} \Delta \lambda}{\left(1 - \frac{\bar{\lambda}_0^2}{\lambda^2}\right)^2} \right] \quad (3)$$

where \bar{n} , $\bar{\lambda}_0$, and \bar{S} are the values averaged over both principal directions (b and a) of the indicatrix section and $\Delta \lambda \equiv \lambda^b - \lambda^a$ and $\Delta S \equiv S^b - S^a$ are the parameters which describe the shift in the oscillator position and strength along both axes. The temperature dependence of the parameters in formula (3) will be discussed in Sec. V.

IV. EXPERIMENTAL RESULTS

A. Experimental procedure

$\text{BAA}(12)\text{-ZnCl}_1$ was obtained by reaction of a stoichiometric mixture of ZnCl_2 and $\text{C}_{12}\text{H}_{25}\text{NH}_3\text{Cl}$ in ethanol. Very high-quality crystals were obtained by slow evaporation according to the methods described by Socías *et al.*²² The chemical composition was checked by chemical analysis and ir spectroscopy.

Birefringence measurements were carried out on monodomain samples by means of a conventional compensator method and an automatized Sernarmont method.²³ The optical arrangement for the latter consists of a polarizer, sample in 45° position, a $\lambda/4$ plate with the fast direction parallel to the polarizer and a rotating analyzer which acts as a modulator and provides the reference signal to a two phase lock-in amplifier. Under these conditions, the measurement of Δn is achieved in a continuous way by monitoring the lock-in phase output as a function of temperature. The light source used in both measuring techniques was a 900-W xenon lamp with a 0.25-m focal monochromator. The same source was also used for conoscopic observations with a microscope set-up on an optical bench. The spectroscopic measurements were performed with a double-beam Cary spectrometer.

B. Birefringence dispersion results

For the birefringence measurements, samples were optically orientated by rotating the crystal platelets about the monoclinic axis (which lies on the layer plane)²⁴ until a biaxial conoscopic pattern centered in the visual field was obtained. Therefore, the measured birefringence corresponds to the difference between two principal crystal indices, one of them corresponding to the direction of the monoclinic axis. During the measuring process neither the extinction directions nor the third principal direction (parallel to the incident light K vector) showed appreciable rotation. Figure 5 shows the temperature and wavelength dependence of the optical path difference for $\text{BAA}(12)\text{-ZnCl}_4$ in the 293–323 K temperature range. The wavelength step between curves is 20 nm. For the sake of clarity only some discrete values of Γ are plotted. Except for a scale factor, optical path differences can be directly identified with Δn values if thermal expansion corrections are neglected. This happens to be our case, since the thermal expansion in the direction normal to the layers is negligible in the temperature interval considered.¹²

As can be observed, birefringence smoothly goes through zero for all scanned wavelengths as temperature is increased. Moreover, the isotropic point shows a spectral dispersion whose temperature dependence is

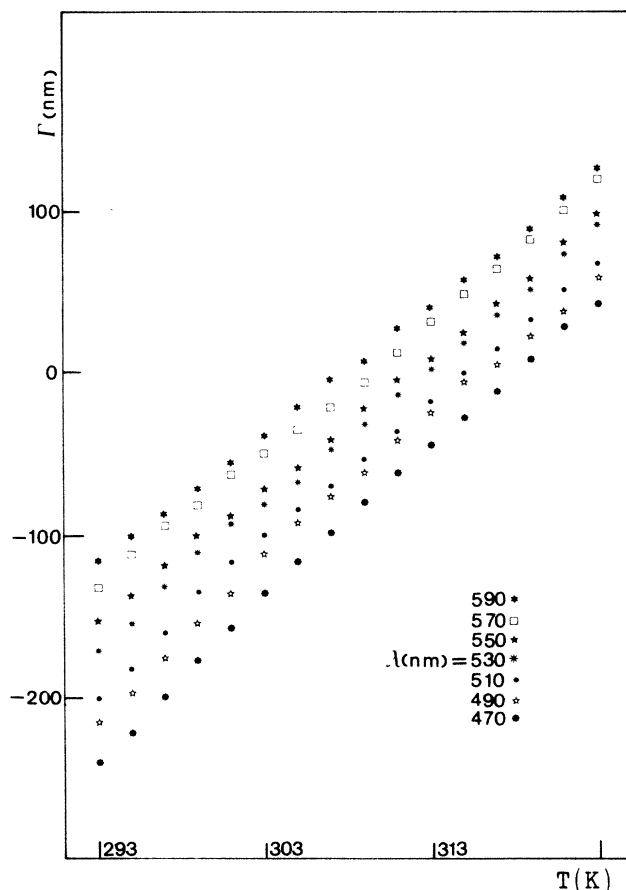


FIG. 5. Temperature and wavelength dependence of optical path difference in $(\text{C}_{12}\text{H}_{25}\text{NH}_3)_2\text{ZnCl}_4$.

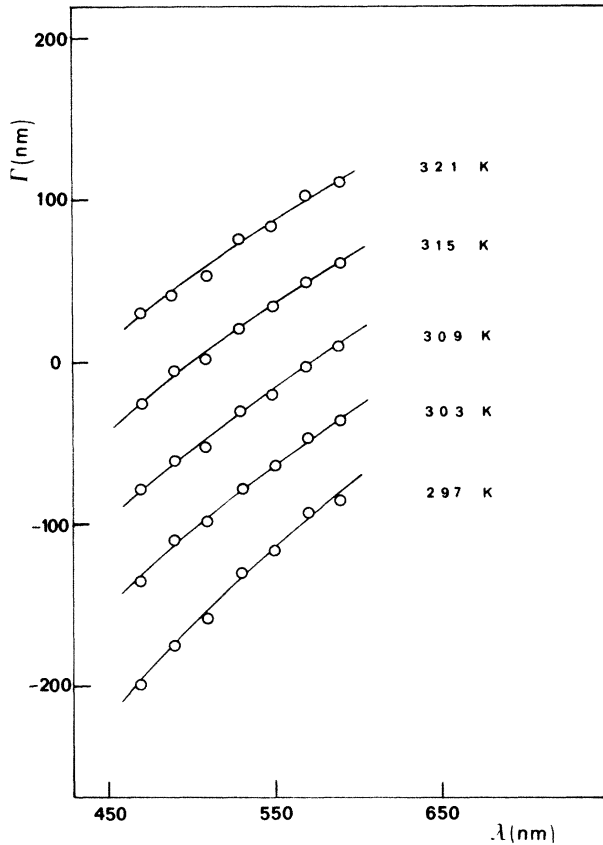


FIG. 6. Best fit of experimental results to Eq. (3).

around 14 nm/K. Figure 6 exhibits the best fit of selected experimental results to equation (3) with three free parameters $\bar{\lambda}_0$, ΔS , and $\bar{S}\Delta\lambda$. Their thermal behavior and physical meaning will be discussed in Section V. As previously stated only some of the experimental points are shown and the selected temperature interval between plotted curves is 6 K.

V. DISCUSSION

A. Optical aspects

Figure 7 shows the values of the fitting parameters $\bar{\lambda}_0$, ΔS , and $\bar{S}\Delta\lambda$ as a function of temperature. As can be seen, all of them exhibit a similar thermal behavior, showing extreme values at about 315 K.

The physical meaning of these parameters in the oscillator model proposed can be found within the frame of the optical band structure. In fact, $\bar{\lambda}_0$ is some average position between the deep intrinsic absorption band and the lowest-energy transfer band. Since the deepest part of the spectrum does not vary noticeably with temperature, the thermal behavior of the wavelength position of the electronic oscillator should be related with that of the low energy transfer band which is roughly represented by the inverse of the energy band gap in Fig. 4. On the other hand, $\bar{S}\Delta\lambda$ in Fig. 7 displays the main features exhibited by the absorption intensity of the lowest ener-

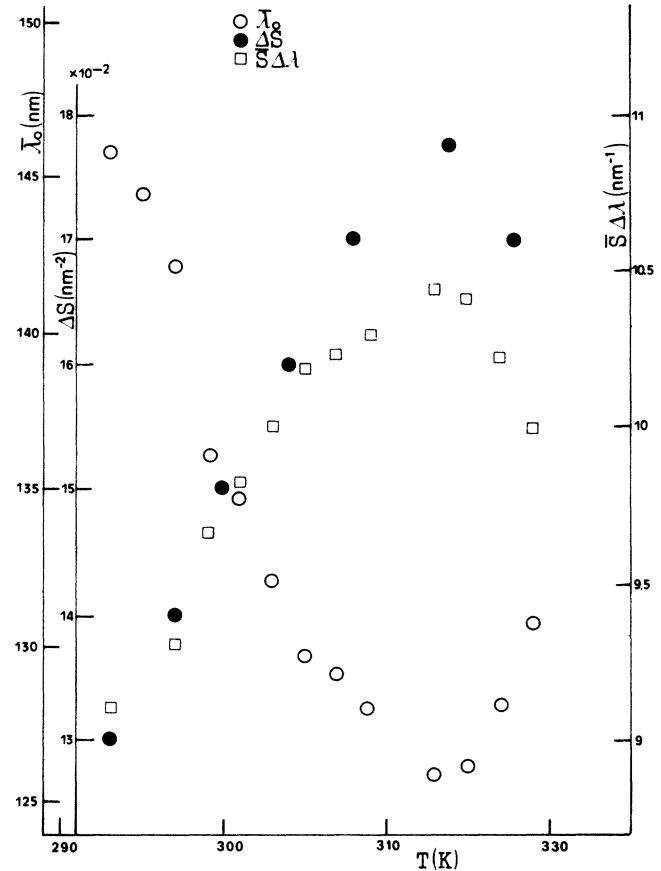


FIG. 7. Fitting parameters $\bar{\lambda}_0$, ΔS , $\bar{S}\Delta\lambda$, as a function of temperature.

gy peak at the absorption edge (Fig. 2). Its negative values are due to $\Delta\lambda$ which is probably not temperature dependent. The behavior of the third parameter ΔS has not been checked by absorption data due to the difficulty to perform spectroscopic measurements with polarized light in this energy range. Nevertheless all the above mentioned facts confirm the adequacy of the selected model and remark the importance of the knowledge of band structure data in supporting the physical interpretation of the parameters involved.

B. Structural aspects around the isotropic point

There is no clear reason for the special behavior displayed by the parameters at 315 K. The obtained results do not imply by themselves the existence of a phase transition at such temperature, but recent measurements of differential scanning calorimetry (DSC) appear to confirm a very slight and diffuse anomaly in that region.²⁵ Similar features are also exhibited by some other members of $BAA(n)\text{-ZnCl}_4$ and $BAA(n)\text{-ZnCl}_2\text{Br}_2$ families in the thermal expansion behavior along the directions parallel to the plates at the corresponding region where the birefringence goes to zero.^{5,25} On the other hand, very complex sequences of phase transitions have been observed and, in some cases, the existence of meta-

stable phases has also been found in the vicinity of the isotropic point.^{5,26,27} This indicates that the free-energy balance is rather subtle at these temperature ranges and the stabilization of a new intermediate phase could not be disregarded. In the present case this hypothetical phase transition should occur at 315 K. It should involve a change of sign in the optical anisotropy of the crystal and would probably connect two monoclinic phases with close lattice energy values. A more detailed

crystallographic study is required to elucidate this point and to clarify the mechanisms responsible for this optical behavior throughout the whole temperature range.

ACKNOWLEDGMENTS

We wish to thank Dr. C. Santiago from Universidad del País Vasco for helpful comments.

-
- ¹L. J. de Jongh and A. R. Miedema, *Adv. Phys.* **23**, 1 (1974).
²R. Geick and K. Strobel, *J. Phys. C* **10**, 4221 (1977).
³R. Blinc, B. Zeks, and R. Kind, *Phys. Rev. B* **17**, 3409 (1978).
⁴R. Kind, R. Blinc, and B. Zeks, *Phys. Rev. B* **19**, 3743 (1979).
⁵J. Fernández, C. Socías, M. A. Arriandiaga, M. J. Tello, and A. López Echarri, *J. Phys. C* **15**, 1151 (1982).
⁶W. Depmeier and S. A. Mason, *Solid State Commun.* **46**, 409 (1983).
⁷J. H. Brunskill and W. Depmeier, *Acta Cryst. Sect. A* **38**, 132 (1982).
⁸P. Muralt, R. Kind, and R. Blinc, *Phys. Rev. Lett.* **49**, 1019 (1982).
⁹R. C. Minteguía, M. J. Tello, J. M. Pérez Mato, A. Gómez-Cuevas, and J. Fernández, *Solid State Commun.* **50**, 501 (1984).
¹⁰F. J. Schafer and W. Kleeman, *Ferroelectrics* **55**, 834 (1984).
¹¹A. Gómez-Cuevas, J. M. Pérez Mato, M. J. Tello, G. Madariaga J. Fernández, A. López Echarri, F. J. Zúñiga, and G. Chapuis, *Phys. Rev. B* **29**, 2655 (1984).
¹²M. A. Arriandiaga, C. Socías, J. Fernández, A. Gómez-Cuevas, M. J. Tello, J. Herreros, and A. López Echarri, *Solid State Commun.* **51**, 477 (1984).
¹³J. Fernández, A. Gómez-Cuevas, M. A. Arriandiaga, and C. Socías, M. J. Tello, *Phys. Rev. B* **31**, 4562 (1985).
¹⁴N. A. Romanyuk, A. M. Kostetsku, V. M. Gaba, A. I. Kits, and V. B. Dunets, *Optical Spectrosc. (URSS)* **50**, (1), 108 (1981).
¹⁵F. J. Zúñiga and G. Chapuis, *Cryst. Struct. Commun.* **10**, 533 (1981).
¹⁶G. Chapuis, K. Schenk, and J. Zúñiga, *Mol. Cryst. Liq. Cryst.* **113**, 113 (1984).
¹⁷J. Zúñiga (unpublished).
¹⁸F. Urbach, *Phys. Rev.* **92**, 1324 (1953).
¹⁹F. Moser and F. Urbach, *Phys. Rev.* **102**, 1519 (1956).
²⁰Di Bartolo, *Optical Interactions in Solids* (Wiley, New York, 1968).
²¹J. B. Marion and M. A. Heald, *Classical Electromagnetic Radiation* (Academic, New York, 1980).
²²C. Socías, M. A. Arriandiaga, M. J. Tello, J. Fernández, and P. Gili, *Phys. Status Solidi (a)* **57**, 405 (1980).
²³J. Etxebarria, I. Ruiz Larrea, M. J. Tello, and A. López Echarri (unpublished).
²⁴M. R. Ciajolo, P. Corradini, and V. Pavone, *Act. Cryst. B* **33**, 553 (1977).
²⁵Socías *et al.* (unpublished).
²⁶J. Zúñiga and G. Chapuis, *Mol. Cryst. Liq. Cryst.* **128**, 349 (1985).
²⁷E. Landi and M. Vacatello, *Thermochim. Acta* **13**, 441 (1975).